Supplemental Material

Full title:

Cargo transport across microtubule intersections: evidence for prolonged tug of war between kinesin motors.

Running head:

Cargo transport across MT intersections

Olaolu Osunbayo*, Jacqualine Butterfield*, Jared Bergman*, Leslie Mershon*, Vladimir Rodionov[#], Michael Vershinin*[†]

* Department of Physics and Astronomy, University of Utah, Salt Lake City, Utah, 84112, USA

[†] Center for Cell and Genome Science, University of Utah, Salt Lake City, Utah, 84112, USA

[#] Department of Cell Biology, University of Connecticut, Farmington, Connecticut, 06030, USA

Fig. S1 Kinesin concentration reference curve. The binding fraction measurements for kinesin bead assays (∅1 μm) were well fit by a single motor curve (red). Motor incubation concentrations used in this study are shown by arrows and stars (* : 0.064 nM ; ** : 0.64 nM). Nominal motor to bead molar ratios were 850:1 and 8500:1 respectively. For comparison with previously published results, note that here kinesin concentration is shown on logarithmic scale.

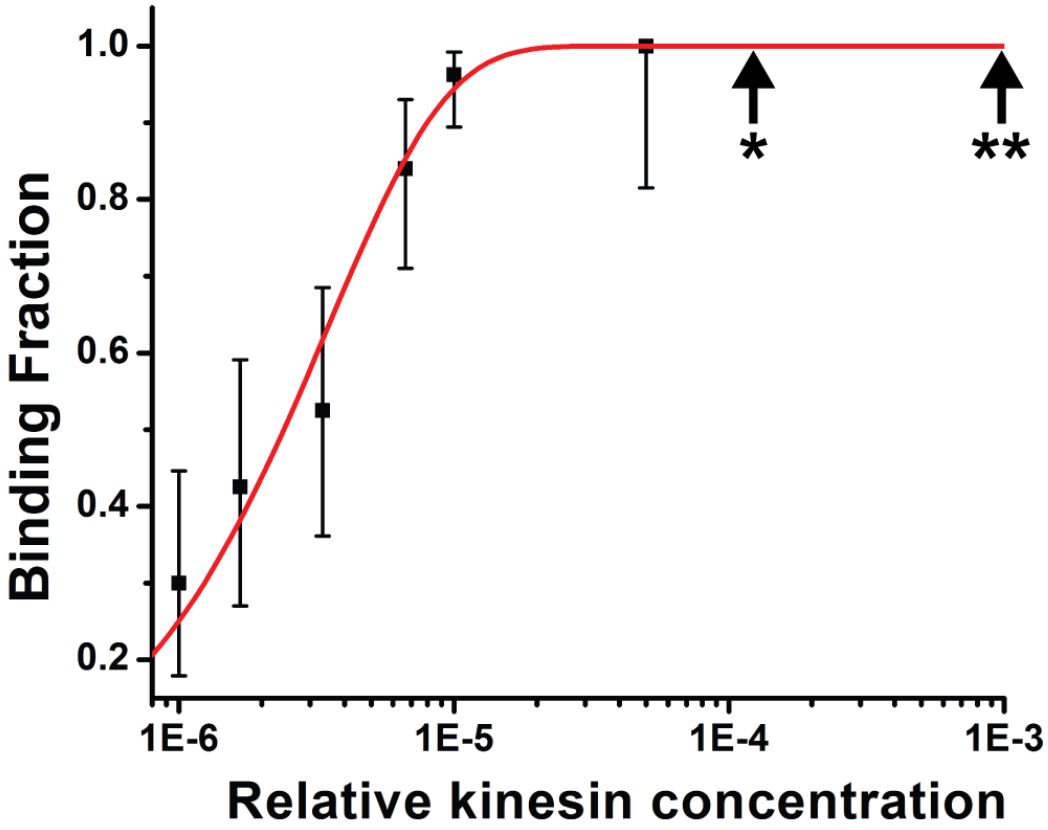

Fig. S2 Cargo velocity when moving along stand-alone MTs. Motor velocities were broadly peaked around 746 ± 51 nm/sec (mean ± SE).

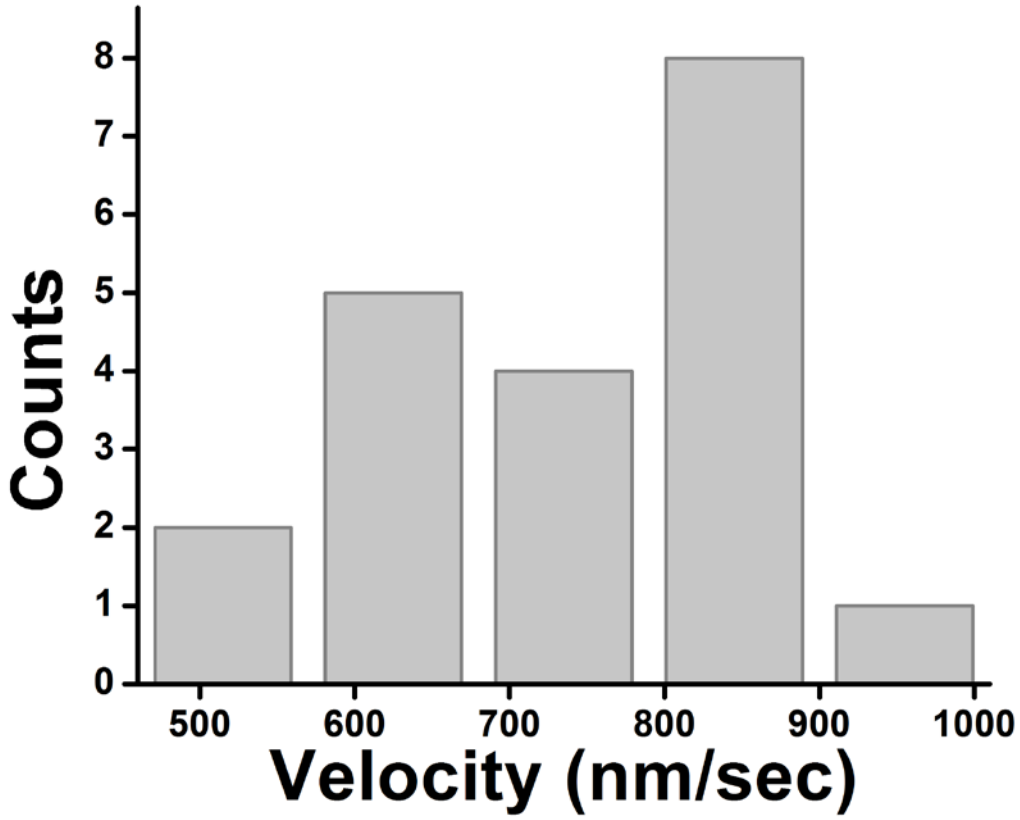

Fig. S3 The angular dependence of dwell times for different size beads. Bead assays for ∅1 μm and ∅3 μm beads were conducted to establish binding fraction curves and in each case an equivalent assay (** in Fig. S1) was used to quantify cargo dwell times ar MT intersections. High motor concentration was chosen to maximize the probability of motor engagement on both MTs during each crossing event and thereby to minimize the probability of undercounting the more localized tug-of-war events. The observed differences were not significant. We observed no evidence that higher bead-MT overlap at intersections (as would be the case for larger beads) leads to a more uniform distribution of dwell times.

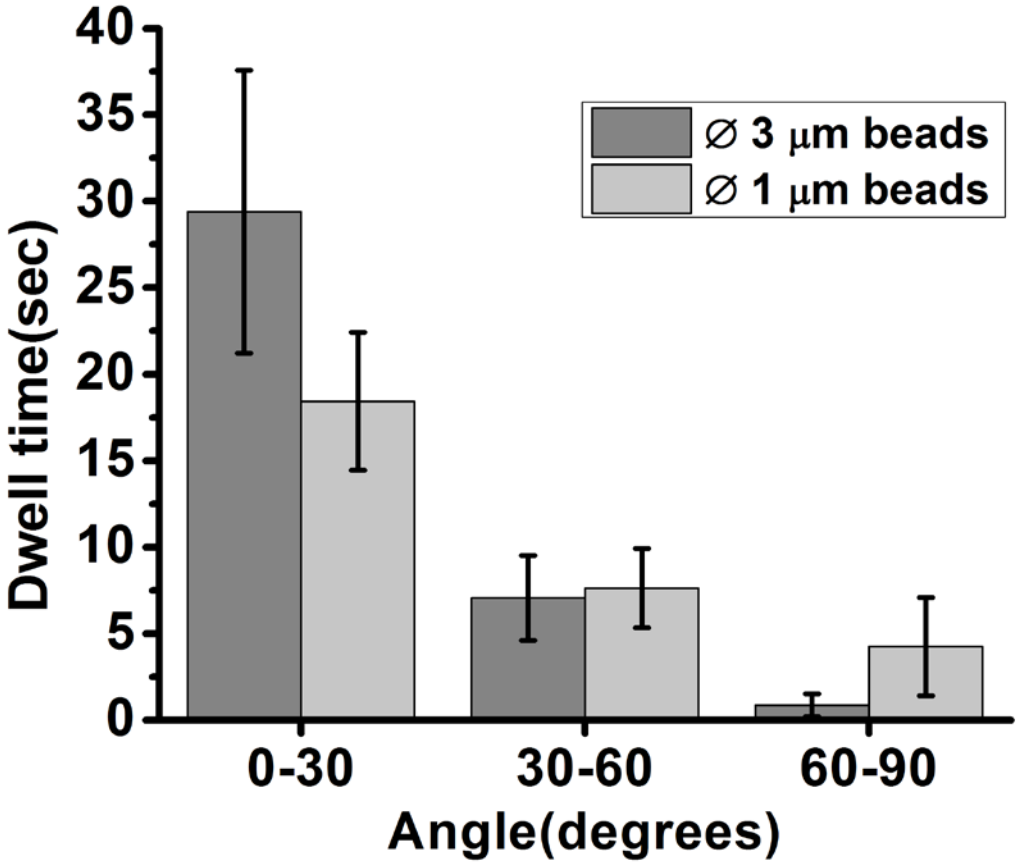

Fig. S4 The effect of MT-MT orientation on dwell times. Dwell times for cargos at intersections for baseline (left, n=59), high motor concentration (middle, n=44) and low salt concentration (right, n=40) assays are shown as a function of MT-MT angle. 180° angle corresponds to parallel MTs with identical polarity.

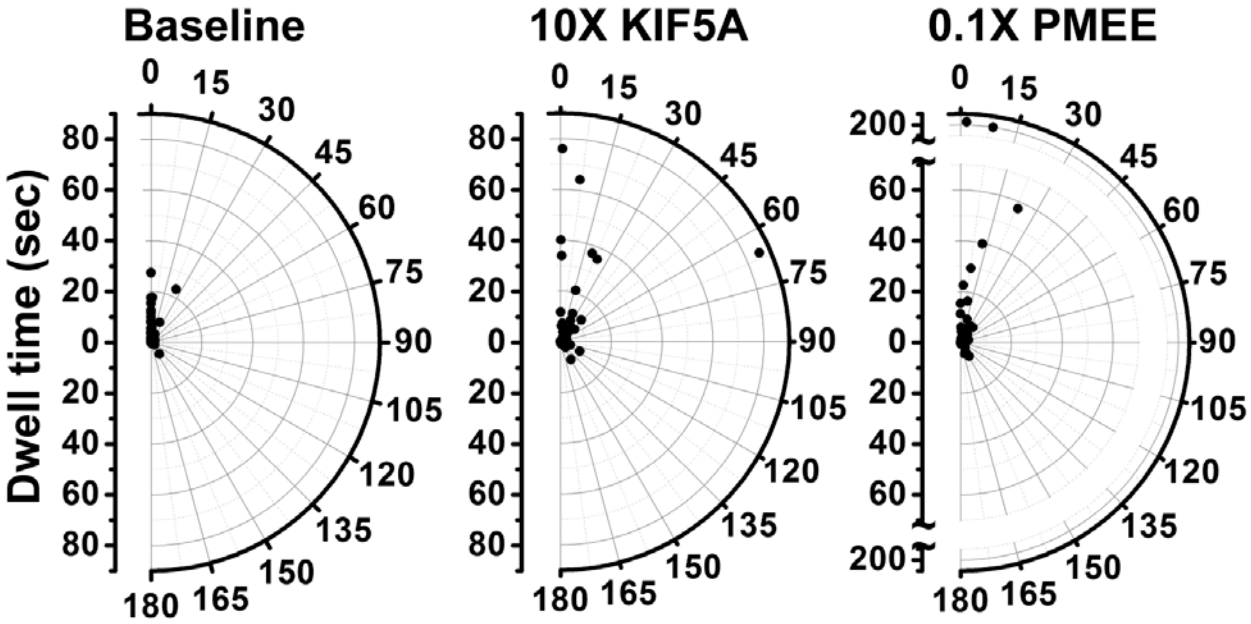

Fig. S5 Histograms of dwell times for intersections of MTs with known polarity. Dwell time distributions lower than 30 s are well fit by exponential decays (red lines) for the baseline, low salt, and high motor concentration assays. See Fig. S4 for angular distribution of these dwell times. Decays times extracted from fits are 3.2±0.4, 4.0±0.8, 5.3±0.4 s (left, middle, right panels respectively). Note that even though an exponential fit is a convenient way to characterize the decay of dwell time distributions, individual motor detachment times are likely to be less than 1 sec – far smaller than the bin size. Therefore it is not possible to tell whether the actual distribution is exponential or e.g. a higher order gamma distribution. We therefore cannot speculate whether single or multiple motor detachment events are associated with termination of dwells.

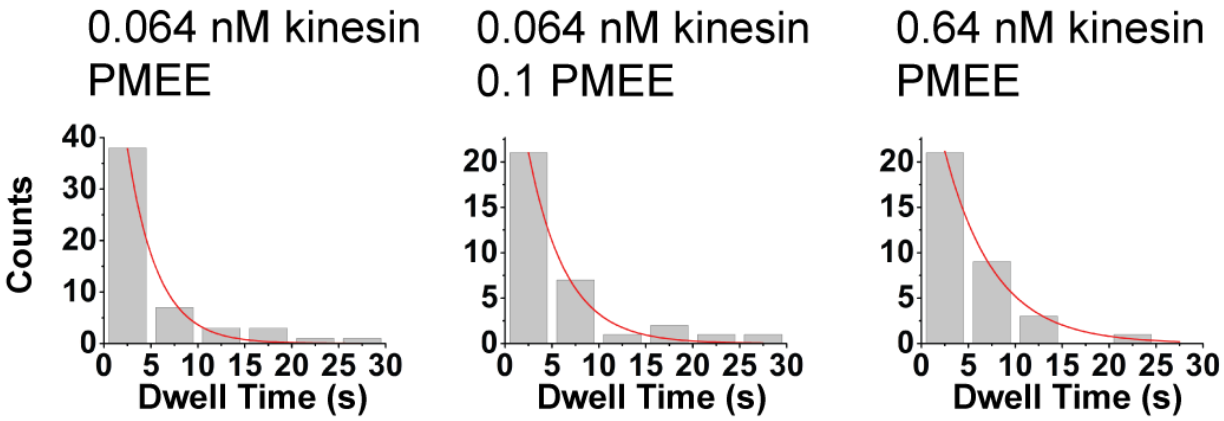

Supplemental Text S1

If cargo dwells at MT crossings are indeed due to opposing action of kinesin motors then one would expect this to occur preferentially for those acute intersection angles where MT polarity was opposite. We therefore attempted to segregate the latter acute angle crossings based on whether MT minus-plus directions were roughly aligned or roughly anti-aligned. We focused on a subset of MT crossings for which cargos switched filaments. In such cases, MT polarity could be inferred for both crossing filaments from the direction of cargo motion, and so the angles between positive directions of MT axes could be quantified.

The crossing angles for known MT polarity cases thus ranged between 0° and 180° rather than 0° to 90° for polarity-agnostic case (Fig. S4). The dwell times for MT crossing angles between 0° and 60° were significantly longer than for higher angles ($p = 0.039$ for baseline assay, $p<0.01$ for high motor and low salt assays). We further examined the 60°-120° range of crossing angles. All pausing events above 4 sec in duration for such crossings involved significant MT deformations. For example, the extreme outlier seen for high motor assay (Fig. S4, middle panel) corresponds to the case where MT crossing had an un-deformed angle of 65.9° but became completely anti-parallel due to cargo activity. The distribution of dwell times for all intersection angles pooled together in all cases was well approximated by an exponential decay (Fig. S5) with a few notable outliers. All outlier events occurred for crossings with nearly opposite MT polarities (0°-30° range), though in the special case discussed above the alignment resulted from MT bending rather than a priori geometry.

Legends to supplemental movies.

Supplemental Movie 1. Cargo motion across an intersection in vivo. Melanosome moving along fluorescently labeled MT in a melanophore encounters another MT, and this encounter leads to buckling of MT that serves as a transport track, and eventual pausing of the melanosome. Numbers indicate time in seconds. Magnification bar is 5 μm.

Supplement Movie 2. Cargo motion across an intersection *in vitro*. An example movie of a crossing event with substantial MT deformation during the crossing. This event corresponds to a sequence of frames shown in Fig. 1B Conformations of MTs before and after the event is comparable. Magnification bar is 2 μm.

Supplement Movie 3. Cargo motion across an intersection *in vitro*. An example movie of a crossing event with a long pause at the intersection during the crossing. This event corresponds to a sequence of frames shown in Fig. 1C. Magnification bar is 4 μm.